Structural investigation of GaInP nanowires using X-ray diffraction

Kriegner, D.; Persson, Johan Mikael; Etzelstorfer, T.; Jacobsson, D.; Wallentin, J.; Wagner, Jakob Birkedal; Deppert, K.; Borgström, M. T.; Stangl, J.

Published in:
Thin Solid Films

Link to article, DOI:
10.1016/j.tsf.2013.02.112

Publication date:
2013

Document Version
Publisher's PDF, also known as Version of record

Thin Solid Films 543 (2013) 100–105

Contents lists available at ScienceDirect

Thin Solid Films

journal homepage: www.elsevier.com/locate/tsf

Structural investigation of GaInP nanowires using X-ray diffraction

D. Kriegner [a,*], J.M. Persson [b], T. Etzelstorfer [a], D. Jacobsson [c], J. Wallentin [c], J.B. Wagner [b], K. Deppert [c], M.T. Borgström [c], J. Stangl [a]

[a] Institute of Semiconductor and Solid State Physics, Johannes Kepler University Linz, Altenbergerstr. 69, A-4040 Linz, Austria
[b] Center for Electron Nanoscopy, Technical University of Denmark, Fysikvej, Building 307, DK-2800 Kgs. Lyngby, Denmark
[c] Solid State Physics and the Nanometer Structure Consortium, Lund University, Box 118, SE-22100 Lund, Sweden

ARTICLE INFO

Available online 5 March 2013

Keywords:
Nanowires
X-ray diffraction
III–V semiconductors

ABSTRACT

In this work the structure of ternary $Ga_xIn_{1-x}P$ nanowires is investigated with respect to the chemical composition and homogeneity. The nanowires were grown by metal–organic vapor-phase epitaxy. For the investigation of ensemble fluctuations on several lateral length scales, X-ray diffraction reciprocal space maps have been analyzed. The data reveal a complicated varying materials composition across the sample and in the nanowires on the order of 20%. The use of modern synchrotron sources, where beam-sizes in the order of several 10 μm are available, enables us to investigate compositional gradients along the sample by recording diffraction patterns at different positions. In addition, compositional variations were found also within single nanowires in X-ray energy dispersive spectroscopy measurements.

1. Introduction

Semiconductor nanowires (NWs) open the possibility to easily combine materials in epitaxial growth, which usually are incompatible due to lattice mismatch [1–3]. This allows more freedom in material choice when designing NW devices in contrast to planar devices, where the difference in the lattice parameter is a limiting factor for the compatibility of materials. For example in electro-optical devices, e.g. solar cells, whose optical absorption spectra need to be tuned to the spectrum of the sunlight for optimal efficiencies [4], the additional freedom gained by the relaxation of the lattice matching criterion, allows for material and hence band gap combinations resulting in higher efficiencies. Especially in solar cells the enhanced absorption of light in NW arrays is advantageous [5,6]. Furthermore, the relaxed lattice matching requirement enables the growth of NWs on relatively cheap group IV substrates such as Si [2,7,8]. For the design of optical devices, the direct band gap of most III–V semiconductor materials is of advantage. In this paper we study the ternary compound $Ga_xIn_{1-x}P$, which has a direct band gap for compositions in the range of $0 \leq x \leq 0.74$, varying between 1.34 eV and 2.26 eV [9]. In NWs it is possible that the limit of $x \leq 0.74$ for a direct band gap can be overcome due to the possibility of GaP growth in the hexagonal wurtzite (WZ) structure. For several materials it was shown that the WZ structure has slightly changed bond lengths and angles in comparison to cubic zincblende (ZB) [10,11], and for GaP it was predicted that those structural change gives rise to a direct band gap [12,13].

Thin film growth of the ternary compound in the full composition range is not feasible on a native substrate because of the lattice mismatch between GaP and InP of more than 7% [9,14]. For NWs, growth parameters in the full composition range could be found for GaInP grown on InP(111)B [15]. However, inhomogeneities of the chemical compositions are present. It is not clear a priori, whether these are gradients within single NWs, fluctuations from NW to NW in the ensemble, or a combination of both effects. The aim of this work is to present techniques to study such composition variations and distinguish between single NW and ensemble effects. For this purpose X-ray diffraction (XRD) and X-ray energy dispersive spectroscopy (XEDS) in a transmission electron microscope (TEM) were used. Due to the fact that the two methods study partly complementary aspects, a combination of both methods is necessary to obtain a complete picture of the chemical composition and crystalline structure present in the samples. The structure of the paper is as follows: After a brief description of the sample growth the applied methods are introduced and the obtained results are shown. We furthermore include a thorough discussion of the XRD based analysis.

2. Experiment

The investigated samples were grown by metal organic vapor phase epitaxy (MOVPE) in particle assisted growth mode. Prior to growth the InP(111)B substrates were decorated by Au-particles of 80 nm diameter with a homogeneous density of 4×10^8 cm^{-2}. As precursors trimethylindium (TMI), trimethylgalium (TMG), and phosphine (PH_3) were used at a pressure of 10 kPa using hydrogen as a carrier gas in a total flow of 6 l/min. In addition to the precursors needed for the GaInP growth, hydrogen chloride was also introduced as an etchant

* Corresponding author.
E-mail address: dominik.kriegner@jku.at (D. Kriegner).

0040-6090/$ – see front matter
http://dx.doi.org/10.1016/j.tsf.2013.02.112

during growth to suppress radial growth and produce non-tapered NWs. The NWs consist of an InP nucleation region, a high band gap GaP barrier to enable optical investigation of the top segment, and the top segment itself, consisting of $Ga_xIn_{1-x}P$ (see Fig. 1c for a schematic of the NW structure). Growth was performed at temperatures of 440 °C, 460 °C and 480 °C using a varying TMI/TMG ratio at constant TMG molar fractions. As an example for the result of such a growth a scanning electron micrograph is shown in Fig. 1a. It shows a sample grown at 460 °C with a TMI/TMG ratio of 1.7. Before growth the initially mono-disperse Au-particles partly coalesce and lead to the formation of a more inhomogeneous ensemble of NWs with diameters ranging from ~40 nm up to above 200 nm. The majority of the NWs however, grow with a diameter close to 80 nm. Fig. 1b shows the sample after removal of the NWs by an ultrasonic bath as discussed below. Details about the sample growth can be found in Ref. [15].

To study the structural parameters of the NW ensembles, X-ray diffraction was used on the as-grown samples. In diffraction, the signal we record includes contributions from the NWs, but also the substrate and possible planar growth between the NWs. Using laboratory XRD tools, average chemical composition as well as compositional ranges in the ensemble of NWs can be detected. Furthermore, the identification of stacking faults and the distinction between the cubic zincblende and the hexagonal wurtzite phase are possible. The measurements were performed with Cu $K\alpha_1$ radiation produced by an optics comprising a parabolic multilayer mirror and a Ge(220) channel-cut monochromator. An area of $\approx 8mm^2$ was illuminated, thus using the nominal area density of NWs more than 30 million NWs contributed to the measured signal.

A position sensitive detector was used to record reciprocal space maps, i.e., the diffracted intensity distribution in a plane in reciprocal space. Although the use of a position sensitive detector speeds up the data collection, it also introduces a certain broadening of the signal which needs to be removed in the data analysis as discussed below.

Reciprocal space maps around the InP $\left(\bar{1}\bar{1}\bar{1}\right)$ reciprocal lattice point were measured in the plane spanned by the $\left[\bar{1}\bar{1}\bar{1}\right]$ and $\left[\bar{1}\bar{1}2\right]$ directions of the substrate. The measured range includes scattering from the InP substrate and all $Ga_xIn_{1-x}P$ alloys up to pure GaP. Furthermore the scattering from the WZ $\left(000.\bar{2}\right)$ reciprocal lattice point [16] would also be observed, since WZ {000.2} planes and ZB {111} planes have nearly the same lattice plane spacing [10,11].

In addition, to better distinguish between WZ and ZB phases, as well as to determine the strain state of the NWs, reciprocal space maps around the asymmetric $\left(\bar{3}\bar{3}\bar{1}\right)$ reciprocal lattice point of the InP substrate up to the respective GaP Bragg peak were recorded. These measurements were extended to include the region of the $\left(\bar{1}01.\bar{5}\right)$ WZ Bragg peaks as well as the position where signals from ZB twinned around the $\left[\bar{1}\bar{1}\bar{1}\right]$ growth direction ($\left(\bar{2}\bar{2}\bar{4}\right)$ Bragg peak) are observed: In ZB crystals, the $\left(\bar{3}3\bar{1}\right)$ and $\left(\bar{2}2\bar{4}\right)$ Bragg peaks occur in azimuths different by 180°. Only one of both peaks can therefore observe in a single azimuth for a perfect crystal. Twins around the [111] direction correspond to a 180° rotation around this direction, so that only for twinned parts of the NWs, the $\left(\bar{2}2\bar{4}\right)$ Bragg peak lies in the same azimuth as the $\left(\bar{3}\bar{3}\bar{1}\right)$ peak [17]. The hexagonal $\left[\bar{1}01.0\right]$ direction is parallel to the cubic $\left[\bar{1}\bar{1}2\right]$ direction, and the WZ $\left\{\bar{1}01.\bar{5}\right\}$ signal has a sixfold symmetry, and is therefore observed in both azimuths. As an example the measurements from NWs grown at 460 °C with a TMI/TMG ratio of 1.7 are shown in Fig. 2. From such measurements the average chemical composition in the ensemble of NWs as well as their strain state and the dominating crystal phase can be determined. In panel (a) the symmetric reciprocal space map showing the diffraction of the {111} (or equivalent hexagonal) lattice planes is seen. Panel (b) shows the diffraction signal from the asymmetrical lattice planes.

Analyzing the asymmetric reciprocal space maps such as the one shown in Fig. 2b we find that all the parts contributing significantly to the diffraction signal are unstrained. This can be seen from the fact that in these measurements the signal is located along the radial direction, as indicated by white lines in the map. The dominating crystal structure in the NWs is identified to be the ZB structure with

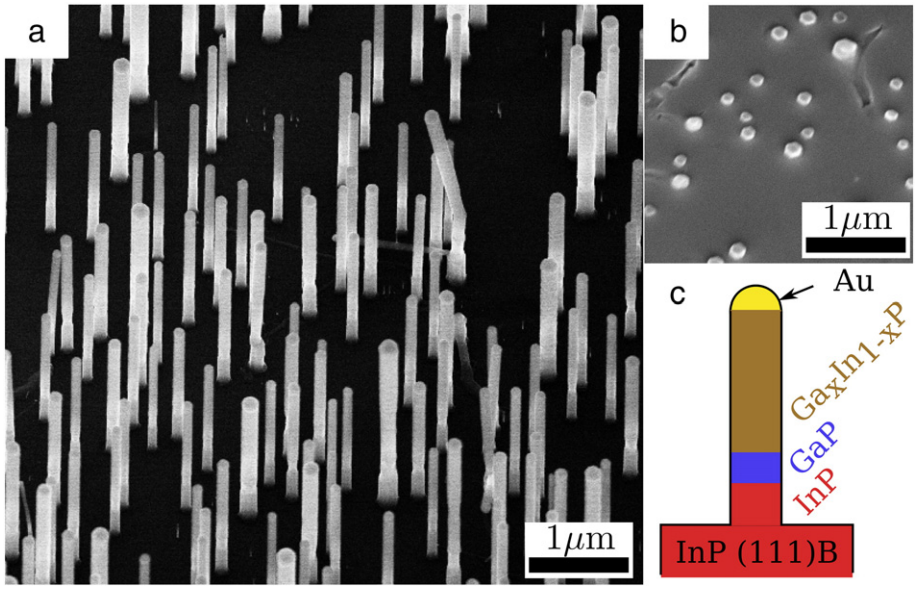

Fig. 1. In panel (a) a scanning electron microscopy image of a sample grown at 460 °C using a TMI/TMG ratio of 1.7 recorded under an angle of 30° is shown. Vertical, non-tapered GaInP nanowires were grown. From the initially mono-disperse Au droplets with a size of 80 nm an inhomogeneous ensemble of nanowires with diameters ranging from ~40 nm to >200 nm evolves. Panel (b) shows a scanning electron micrograph of a sample after removal of the wires by an ultrasonic bath. Panel (c) shows the nominal structure of a nanowires grown on InP(111)B substrates.

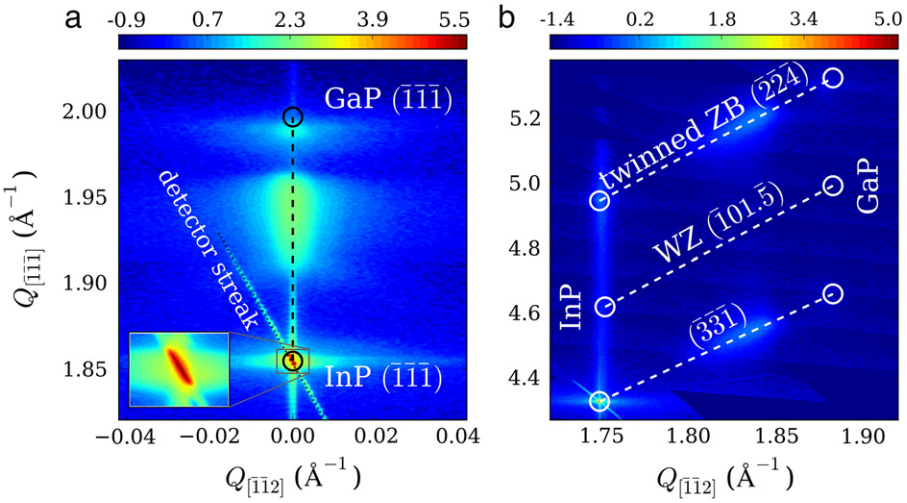

Fig. 2. X-ray diffraction reciprocal space maps of a sample grown at 460 °C with a TMI/TMG ratio of 1.7 showing the logarithmic scattering intensity. In panel (a) the reciprocal space map around the $(\bar{1}\bar{1}\bar{1})$ Bragg peaks is shown. Black circles mark the nominal position of InP and GaP. Furthermore an artifact from the measurement, the detector streak, is indicated by a dotted line and the broadening due to the finite beam size is shown in the inset. In panel (b) the reciprocal space map including the InP, GaP $(\bar{3}\bar{3}\bar{1})$, WZ $(\bar{1}01.\bar{5})$ and $(\bar{2}\bar{2}\bar{4})$ Bragg reflections is shown. White circles mark the nominal positions of InP and GaP.

both twin orientations. A signal of a WZ phase is only found for the InP nucleation region, where a $(\bar{1}01.\bar{5})$ peak is observed, which is, however, much weaker than the zincblende $(\bar{2}\bar{2}\bar{4})$ peak. For the GaInP segment, no $(\bar{1}01.\bar{5})$ WZ Bragg peak is found at all.

To determine the chemical composition of the NWs line cuts need to be extracted from the reciprocal space maps along the radial direction, i.e. along the line connecting the origin of reciprocal space with the respective Bragg peak of interest. We used the $(\bar{1}\bar{1}\bar{1})$ Bragg reflection, which is insensitive to twin defects. The width of the obtained peaks in the line scans along $[\bar{1}\bar{1}\bar{1}]$ shown in Fig. 3a depends on several factors: (i) the finite size of scattering objects gives rise to a Bragg peak width inversely proportional to that size. (ii) Strain gradients in the scattering objects, which are, however, not relevant here, as the NWs are unstrained. (iii) Distributions of the chemical composition and hence lattice parameter lead to a "smearing" of the Bragg peak. (iv) The instrumental resolution results in a lower limit of the Bragg peak width. In nanostructures the resolution effect (iv) can usually be neglected in comparison to size effect (i). However, the GaInP segment length is in the micrometer range, and the corresponding peak width is smaller than the experimental resolution, which can be seen in the inset of Fig. 2a [18]. In order to exclude any resolution effects in the analysis, we therefore performed a deconvolution of the experimental data with the resolution function. The result of such a deconvolution in comparison with the raw data is shown in Fig. 3a. It has an effect mostly close to the substrate peak and results in a steeper decay of the GaInP signal. The main peak of GaInP is rather broad and not affected by the deconvolution.

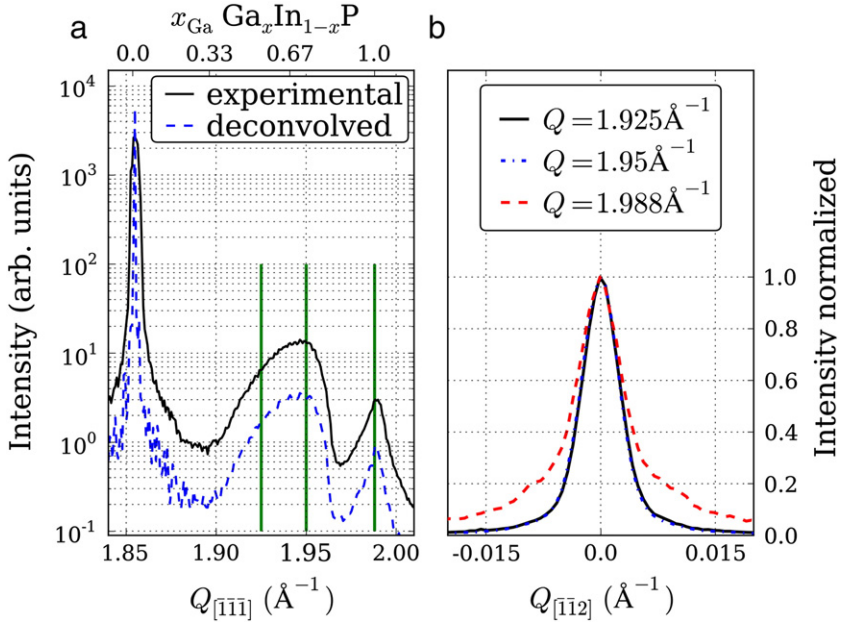

Fig. 3. X-ray diffraction line cuts through the reciprocal space map shown in Fig. 2a. In panel (a) the line cuts along the $[\bar{1}\bar{1}\bar{1}]$ direction are shown. To obtain those line cuts the intensity was summed up along the perpendicular $[\bar{1}\bar{1}2]$ direction. Vertical lines mark the position where line cuts along the $[\bar{1}\bar{1}2]$ direction were done. These line cuts are shown normalized to their maximum in panel (b). The two line cuts through the $Ga_xIn_{1-x}P$ signal are virtually the same when normalized. The third line cut through the GaP-rich signal is significantly broader.

Finite size effects are of importance in the lateral direction, i.e. across the NW diameter in $[\bar{1}\bar{1}2]$ direction. Cuts along this direction are shown in Fig. 3b for different momentum transfers as indicated in panel (a). Notable is that the peak width of the GaP-rich barrier segment is found to be ~20% larger than the width of the GaInP peak. This means that the GaP segments are thinner than the GaInP segments grown on top. Indeed this is also observed in electron microscope investigations for several samples (see Figs. 1a and 6a).

The remaining cause for the peak broadening along $[\bar{1}\bar{1}\bar{1}]$ direction is effect (iii), a variation in chemical composition. Therefore, we can convert the abscissa in Fig. 3a from $Q_{[111]}$ to x_{Ga}. To do so we use Vegard's rule [19] and obtain

$$x_{Ga} = \left(\frac{2\pi}{Q_{[111]}}\sqrt{3} - a_{InP}\right)/(a_{GaP} - a_{InP}), \quad (1)$$

valid for unstrained ZB NWs with the bulk lattice parameters of InP and GaP from Ref. [20]. To highlight the importance of the knowledge of the crystal phase, we note that the slight change in lattice plane spacing introduced by the change from the cubic to the hexagonal stacking leads to an error in the chemical composition of ~5% [21].

For a series of samples grown at different TMI/TMG ratios (r) such a plot is shown in Fig. 4. Since stacking defects, e.g. twin defects, do not affect the symmetric $(\bar{1}\bar{1}\bar{1})$ Bragg peak we can associate the amount of material present in the samples with the integrated intensity, which is actually proportional to the square of the scattering volume. To adjust the weights in the plot accordingly, we plot the intensity on a square root scale versus the chemical composition. The signal close to the substrate is omitted in those plots because the presented approach is only valid for the nanostructures on the surface, which are illuminated by a quasi constant intensity, i.e. absorption can be neglected. Clearly the shift of the chemical composition upon a change of the precursor ratio is observed, however, for all samples a compositional range of 20% or more was found. The signal of the GaP barrier is seen only as very weak signal due to the rather small extensions of this segment. Note, however, that it is clearly visible in the logarithmic scale in Fig. 3. For one sample ($r = 2.93$) the composition distribution between 38 and 58% is rather homogeneous, whereas for others the distribution is more complicated. To prove that the signal we recorded is arising exclusively from the NWs and not from probably existing parasitic surface growth, for which indications were found in TEM, the XRD measurements were repeated after the removal of the NWs. For this purpose the samples were submerged into an ultrasonic bath for several minutes. SEM revealed that after such a treatment only short NW trunks and traces along the surface due to a "movement" of catalyst particles which did not initiate vertical NW growth remained, see Fig. 1b. Since the NW trunks consist of InP, the corresponding XRD signal is merged with the substrate scattering. No other signal is observed from the sample after the ultrasonic treatment, as seen in Fig. 4 (dashed line). Hence, the GaInP signal arises exclusively from the NWs, and any surface layer which might be present is therefore not influencing our analysis. From the XRD data we can, however, not distinguish between an ensemble of NWs with different compositions and a composition gradient within single nanostructures. Even for ensemble effects, there might be different types of variation: either a "random" fluctuation of composition from NW to NW, or a gradual change in composition across the sample.

This would mean that locally the NWs possess rather similar chemical composition, and only due to the fact that the composition varies across the sample surface the signal in XRD is spread. To test this hypothesis synchrotron X-ray diffraction measurements using a beam of 40 μm diameter were done at different positions of a sample at beamline ID01 at ESRF, Grenoble. Due to projection of the beam at sample angles of 12° to 13° the beam footprint on the sample at the $(\bar{1}\bar{1}\bar{1})$ Bragg peak is approximately $40 \times 180\ \mu m^2$. In a beam spot of this size, still more than 20,000 NWs are illuminated. The radial scattering curves recorded along the $[\bar{1}\bar{1}\bar{1}]$ direction are shown in Fig. 5. The same measurement was performed at four distinct positions with a distance of 600 μm. Every single measurement already shows a rather broad signal (~ 20% variation) arising due to a chemical composition distribution present in the illuminated sample area. In addition to this, also a shift of the signal is observed between the measurements at different positions. The observed chemical compositions on this sample span the range between 35 and 70% of Ga. In comparison the laboratory measurement looks similar to the sum of the synchrotron measurements, which is also expected, since almost the whole sample surface is illuminated in the laboratory experiments.

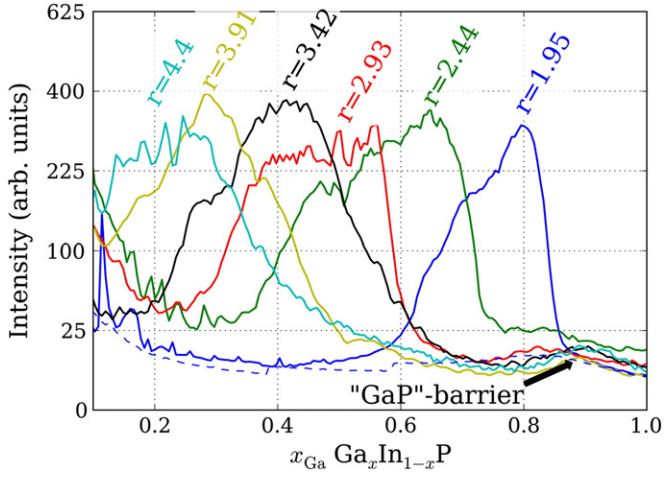

Fig. 4. Scattered intensity on square root scale plotted versus the chemical composition determined from the reciprocal space position around the $(\bar{1}\bar{1}\bar{1})$ Bragg peak. It shows the different chemical compositions present in the nanowire ensembles. Intensity curves for samples grown at 480 °C using different TMI/TMG ratios (r) are shown. The ratio r influences the average chemical composition in the nanowires. For all samples we observe gradients in the chemical composition of 20% and more within the illuminated spot-size of $\approx 2 \times 4$ mm^2. The GaP-rich barrier shows up as weak signal at $x_{Ga} \sim 0.9$. In addition a dashed line shows the measurement performed after removal of the NWs.

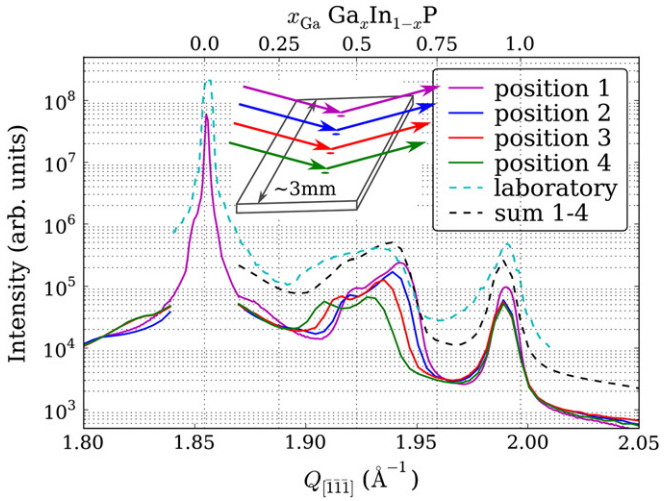

Fig. 5. Synchrotron X-ray diffraction line cuts measured at a sample grown at 440 °C using a TMI/TMG ratio of 0.4. The measurements were done using a circular X-ray beam with diameter of 40 μm at different positions on the same sample. The projection of the beam spot into the sample surface is indicated by the ellipse shown in the inset. In addition the sum of the synchrotron measurements and the line cut obtained from laboratory measurements using a beamsize of several millimeters is shown.

To further clarify the origin of the chemical broadening, XEDS measurements of single NWs were performed in an FEI Titan 80–300 at 300 kV, with an Oxford INCAx-sight detector in scanning TEM mode. Therefore the NWs were moved to a carbon grid by mechanical transfer before investigation. As a consequence, the substrate and the nucleation regions of the NWs are not seen using this procedure. The probe size is in the sub-nm regime in this instrument, but was spread slightly to prevent irradiation damage of NWs containing phosphorous. However, probe sizes were kept well below 5 nm in all cases with collection times in the order of 10 s per position. The composition was studied along the NW axis by collecting electron beam induced X-ray fluorescence data repeatedly along a line in the center of the NW. In order to analyze sharp interfaces all measurements were performed at the [110] zone axis, though slightly tilted away in order to avoid channeling effects. The data was analyzed using the proprietary software TIA (TEM Imaging and Analysis) provided by FEI. Due to the very-time consuming procedure only selected samples were investigated by XEDS. For most samples three randomly chosen NWs were used for detailed study.

The resulting spectra show that there is a large variation of the chemical composition, both between NWs within the same sample and for some samples also within the NWs, see Fig. 6a. Local variations in crystal structure could help explain the variation within individual NWs. Abrupt changes of the chemical composition are always observed concomitantly with stacking defects. In some cases even stacking faults in the $\left(11\bar{1}\right)$ planes are observed, which prohibit any other defects in the {111} planes [15]. In Fig. 6b a comparison between the chemical composition found within a single NW investigated with XEDS and the ensemble XRD measurement is shown. The shown NW exhibits a large variation in x_{Ga}. While this was a rather typical measurement, a NW with a smaller compositional variation was also found in the same sample.

Most obtained XEDS signals overlap with the range observed in XRD, however, in the XEDS scan shown in Fig. 6, even slightly higher x_{Ga} values were found. We attribute this to the fact that it is not known from which part of the sample a NW investigated in XEDS is originating. This area must not necessarily be the same as the one investigated in XRD.

3. Discussion

Combining the results obtained by the different techniques, we can conclude that a variation of the chemical composition is present in single NWs as well as in the ensemble of NWs. Long range gradients of the Ga content in the order of 10% have been detected, while short range fluctuations on a length scale of few 10 μm are of the order of 20%. Variations within single NWs have been detected as well, with a rather large scatter of values between few % and up to 30%. The found local variation of the chemical composition is also consistent with photoluminescence (PL) studies [15]. In those PL studies, where only ~200 NWs are illuminated, also a broad emission signal is found, whose width corresponds to 8% variation in chemical composition [15]. However mostly the NW segments with smaller band gap contribute in those measurements due to diffusion of carriers into the low band gap segment of each NW. The reasons for the composition fluctuations on various length scales cannot be completely separated from the investigated set of samples. The long-range gradients across each sample may be connected to gradients in the precursor concentrations in the MOVPE reactor. Short range fluctuations from NW to NW are most probably the result of size fluctuations of the catalytic particles, together with local variations of NW density. The observed x_{Ga} variation within individual NWs may be connected to the supersaturation of the different elements in the catalytic particle, which can change during growth due to finite surface diffusion lengths of the different species. More detailed insight into the growth processes could be obtained for a set of samples, where some of the mentioned parameters are well controlled. For instance, growing NWs from a regular pattern of catalyst particles fabricated, e.g., by lithography, could eliminate the local variations of catalyst particle size and density.

The combination of methods presented above provides a powerful tool to analyze the resulting variations and gradients on different length scales. For variations within single NWs, XEDS is certainly the method of choice. Since the original location of individual NWs on the sample is not known, complementary methods are required. X-ray diffraction data recorded for different illuminated areas do provide this information. Furthermore, XRD can also obtain data from the NW nucleation regions, which are missing in NWs transferred to TEM grids. To assess these regions in TEM, a cross sectional lamella would need to be prepared. During the preparation process, comprising mechanical polishing and ion milling, NWs easily break off, so that only a random subset of NWs remains for characterization. Hence the combination of XEDS and XRD seems to be the most appropriate method in order to perform a comprehensive analysis of composition variations.

In summary, we presented methods to analyze alloy semiconductor nanowire samples with respect to their chemical composition homogeneity. Therefore GaInP nanowires grown by metal organic vapor phase epitaxy were investigated. X-ray diffraction was used to analyze the samples in the as-grown state, where large ensembles of NWs are investigated at the same time. Variations of the chemical composition in

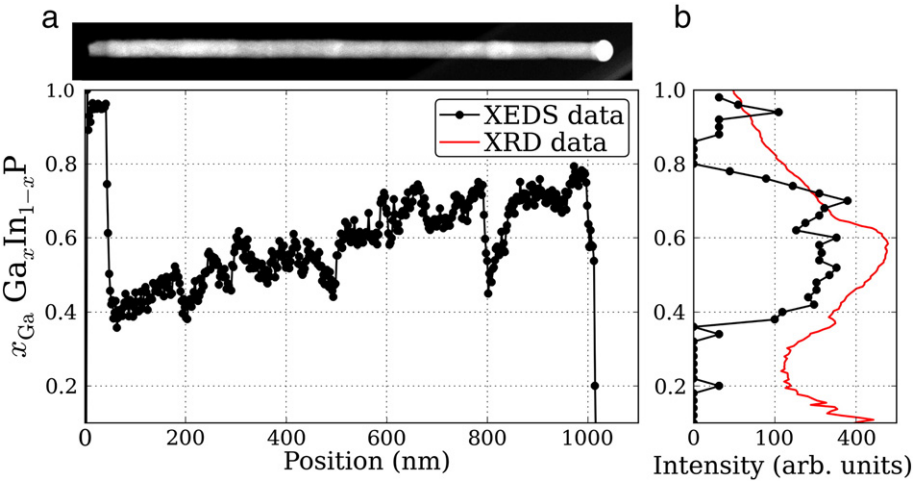

Fig. 6. Panel (a) shows a STEM image and x_{Ga} as obtained from an XEDS line scan along a nanowire from a sample grown at 460 °C using a TMI/TMG ratio of 1.47. Abrupt changes of the chemical composition are observed at positions where stacking defects can also be seen in TEM images. In panel (b) a comparison of the chemical composition as found for the particular nanowire investigated in TEM (black dots) and the ensemble XRD measurement (red line) of the same sample is shown.

the range of 20 to 30% with complicated distribution functions were found. Synchrotron based diffraction investigations revealed that the chemical composition varies across the sample surface. Complementary to the diffraction based investigations, X-ray energy dispersive spectroscopy was used to study the local variations within single nanowires. Variations of the chemical composition were found within the nanowires along the growth direction. Stacking defects were found to lead to abrupt changes of the chemical composition. Combining the results from the local XEDS investigations and ensemble XRD measurements a complete picture of the chemical composition is obtained.

Acknowledgments

The authors thank M. Keplinger and M. Steindl for fruitful discussions and the staff at ID01 ESRF (R. Grifone and T. Schülli) for the assistance with the beamline setup. We acknowledge the financial support from FWF Vienna (SFB025 IR-ON) and the EC (AMON-Ra, 214814). D.K. acknowledges financial support by the Austrian Academy of Science. Part of this work was supported by the Nanometer Structure Consortium at Lund University (nmC@LU), the Swedish Foundation for Strategic Research (SSF), the Swedish Research Council (VR), Swedish Energy Agency, and the Knut and Alice Wallenberg Foundation. We gratefully acknowledge the use of the TEM facilities at the Center for Electron Nanoscopy at the Technical University of Denmark.

References

[1] Frank Glas, Phys. Rev. B 74 (12) (2006) 121302.
[2] Erik P.A.M. Bakkers, Magnus T. Borgström, Marcel A. Verheijen, MRS Bull. 32 (2007) 1, (February).
[3] Karen L. Kavanagh, Semicond. Sci. Technol. 25 (2) (2010) 024006.
[4] A. De Vos, J. Phys. D 13 (5) (2000) 839.
[5] Jan Kupec, Ralph L. Stoop, Bernd Witzigmann, Opt. Express 18 (26) (2010) 27589.
[6] N. Anttu, H.Q. Xu, J. Nanosci. Nanotechnol. 10 (11) (2010) 7183.
[7] C. Patrik T. Svensson, Thomas Mårtensson, Johanna Trägårdh, Christina Larsson, Michael Rask, Dan Hessman, Lars Samuelson, Jonas Ohlsson, Nanotechnology 19 (30) (2008) 305201.
[8] Katsuhiro Tomioka, Junichi Motohisa, Shinjiroh Hara, Takashi Fukui, Nano Lett. 8 (10) (2008) 3475.
[9] P. Merle, D. Auvergne, H. Mathieu, J. Chevallier, Phys. Rev. B 15 (4) (1977) 2032.
[10] M. McMahon, R. Nelmes, Phys. Rev. Lett. 95 (21) (2005) 215505.
[11] D. Kriegner, E. Wintersberger, K. Kawaguchi, J. Wallentin, M.T. Borgström, J. Stangl, Nanotechnol 22 (42) (2011) 425704.
[12] A. De, Craig E. Pryor, Phys. Rev. B 81 (15) (2010) 155210.
[13] Abderrezak Belabbes, Christian Panse, Jürgen Furthmüller, Friedhelm Bechstedt, Phys. Rev. B 86 (7) (2012) 75208.
[14] G.B. Stringfellow, Organometallic Vapor-phase Epitaxy: Theory and Practice, Elsevier Science, 1999.
[15] D. Jacobsson, J.M. Persson, D. Kriegner, T. Etzelstorfer, J. Wallentin, J.B. Wagner, J. Stangl, L. Samuelson, K. Deppert, M.T. Borgström, Nanotechnology 23 (24) (2012) 245601.
[16] We use the Miller indices (*hkl*) to denote cubic and Bravais indices (*hki.l*) with $i = h - k$ to denote the hexagonal WZ structure.
[17] D. Kriegner, C. Panse, B. Mandl, K.A. Dick, M. Keplinger, J.M. Persson, P. Caroff, D. Ercolani, L. Sorba, F. Bechstedt, J. Stangl, G. Bauer, Nano Lett. 11 (4) (2011) 1483.
[18] Beside a finite beam divergence and angular detector resolution the beam size in real space leads to a finite peak width when a position sensitive detector is used. The latter is especially important in laboratory experiments where beam sizes are rather large and detector distances are moderate.
[19] L. Vegard, Z. Phys. 5 (1921) 17.
[20] http://www.ioffe.ru/SVA/NSM, (accessed April 2012).
[21] To obtain the shown value a lattice parameter deviation due to the change from the cubic to hexagonal stacking equal to the one given in Ref. [11] for InP was assumed.